JOURNAL OF PROPULSION AND POWER
Vol. 25, No. 4, July–August 2009

Oxygen/Hydrogen–Planar-Laser-Induced Fluorescence Measurements and Accuracy Investigation in High-Pressure Combustion

Aravind Vaidyanathan*
Iowa State University, Ames, Iowa 50011
and
Jonas Gustavsson† and Corin Segal‡
University of Florida, Gainesville, Florida 32611

DOI: 10.2514/1.39013

Inflow species concentration measurements in reacting flows at high pressures, based on nonintrusive methods, have been acquired so far for isolated conditions in a range of experimental devices and by using a variety of methods. Furthermore, extensive assessments of the uncertainties associated with the measurement techniques are lacking. In general, these methods have been based on calibrations determined from assumptions that were not sufficiently quantified to provide a detailed range of the uncertainties associated with these measurements. This work quantifies the uncertainties associated with OH measurement in an oxygen–hydrogen system produced by a shear, coaxial injector typical of those used in rocket engines. Planar OH distributions are obtained for a range of pressures from 10 to 53 bar, providing instantaneous and averaged distribution in a unified study, using the same experimental setup and maintaining the rest of the parameters the same. The uncertainty of 18 different parameters was evaluated and the overall root mean square error was found as 21.9, 22.8, 22.5, and 22.9% at 10, 27, 37, and 53 bar, respectively.

I. Introduction

FUTURE power systems for flight or ground applications will increasingly rely on computational fluid dynamics (CFD) as design tools. They will require, in turn, reliable experimental validation data. To date, this database is still limited [1]. Generally, high-pressure data are scarce and, in particular, uncertainty analysis is rarely addressed. Among the targeted inflow measurements, OH is of major importance because it serves as a marker of the near-stoichiometric high-temperature flame zone [2–4]. A set of experimental studies that focused on the inflow species measurements for coaxial injectors in the past 10–15 years [4–21] is shown in Table 1, indicating the extent of uncertainty evaluation and, when included, the value of these uncertainties. This review clearly indicates that a thorough uncertainty analysis is still needed to improve the quality of the inflow measurements for CFD validation.

The diagnostic methods used in the previous rocket injector studies included Raman spectroscopy for H_2O, H_2, and O_2 mole fraction measurements and OH emissions and planar-laser-induced fluorescence (PLIF) for visualization. As an example, Singla et al. [4] recently provided semiquantitative OH distribution for gaseous hydrogen/liquid oxygen (GH_2/LOX) cryogenic flames at 60 bar without converting signal intensities to the actual number density. Potential error sources which typically originate from shot noise, spatial variation in laser sheet intensity profiles, and laser shot-to-shot power fluctuations were not addressed. It can be seen from Table 1 that only 4 out of 18 previous experimental studies addressed and included a limited number of uncertainty factors associated with the measurements. Quantitative OH measurements with detailed uncertainty analysis for gaseous H_2/O_2 (GH_2/GO_2) systems at high pressures, which are of particular interest for current code development of rocket engines, are scarce. Validation of gaseous systems is of interest as a preliminary step before developing the more challenging liquid-fuel-based reacting computational capabilities. Hence, the current work is aimed at providing inflow quantitative OH measurements for a single element, shear coaxial GH_2/GO_2 injector at pressures in excess of 50 bar, including detailed uncertainty analysis.

Laser-induced fluorescence (LIF) techniques have been used for species concentration measurements in a wide range of environments. Hanson [22], for example, provided a detailed review of the application of planar imaging of fluorescence, giving examples of PLIF application to obtain species concentration, 2-D temperature fields, velocity, and pressure imaging. Several research groups have successfully applied LIF to obtain OH species concentration in harsh combustion environments [23–25]. The majority of these studies were carried out at pressures below 20 bar; at high pressures, quantitative OH data are limited.

The results of the present study from low to high pressure, including 10, 27, 37, and 53 bar are described next, followed by a detailed uncertainty analysis of 18 parameters involved in these measurements.

II. Experimental Technique, Facility Description, and Instrumentation Layout

A. Laser-Induced Fluorescence: Quantitative Method

Fluorescence modeling has been discussed previously and will not be reviewed here; detailed explanations are given by Eckbreth [26] and others [4,24,27]. A mathematical formulation of all the processes involved in the linear fluorescence regime of A-X(1,0) transition is made to infer target species number density as

Received 9 June 2008; revision received 23 December 2008; accepted for publication 11 January 2009.

*Post Doctoral Research Associate, Department of Mechanical Engineering. Member AIAA.
†Post Doctoral Research Associate, Department of Mechanical and Aerospace Engineering. Member AIAA.
‡Associate Professor, Department of Mechanical and Aerospace Engineering; cor@ufl.edu. Associate Fellow AIAA.

$$n^0_{\mathrm{OH}} = \frac{N_p}{(E/A_{\mathrm{laser}})\{(\sum_1^9 f_B B_{12}/c^2)(\int \Phi_{\mathrm{laser}}\Phi_{\mathrm{abs}}\,\mathrm{d}\nu)[A_{21}/(A_{21}+Q_{21})]\}[V\eta(W/4\pi)]} \quad (1)$$

Here N_p is the number of photons detected, n^0 is the number density (cm^{-3}) of the target species, E is the laser energy per pulse (Joule), A_{laser} (cm^2) is the area of cross section of the laser beam/sheet, f_B is the Boltzmann factor of the transition excited, B_{12} is the Einstein $\boldsymbol{B}$ coefficient for absorption ($\mathrm{cm}^3\ \mathrm{J}^{-1}\ \mathrm{s}^{-2}$), c is the speed of light (cms^{-1}), $\int \Phi_{\mathrm{laser}}\Phi_{\mathrm{abs}}\,\mathrm{d}\nu$ is the overlap integral (centimeters), $A_{21}/(Q_{21}+A_{21})$ is the fluorescence yield, V (cm^3) is the volume probed by the laser, η is the efficiency of the detection optics and camera, and $\Omega/4\pi$ is the fraction of solid angle detected. The term

$$\sum_1^9 f_B B_{12}/c^2$$

referred to as

$$\sum_1^9 f_B B'_{12}$$

includes the contributions of the nine rovibrational lines that are employed for OH-PLIF in the current study. The absorbing species line shape function $\Phi_{\mathrm{abs}}(\upsilon)$ is simulated using LIFBASE as described in literature [4,26–29]. The fluorescence yield was calculated as described in detail by Paul [30] and Singla et al. [4].

The physical significance of the terms from the experimental, modeling, and quantifying point of view are shown in Fig. 1.

The excitation and detection strategy of OH consists of the A-X (1,0) transition in the current study. The detection electronics used to collect fluorescence was an intensified charge-coupled device (ICCD) camera. There are interference effects from other species present in the combustion environment, elastic scattering, and the background emissions.

The laser pulse energy employed in PLIF measurements and the shot-to-shot power fluctuation needs to be monitored. The laser beam/sheet profile is nonuniform in space and needs to be corrected for quantitative measurements. The laser beam is attenuated as it

Table 1 Previous experimental studies on rocket injectors

Ref.	Injector type	P, bar	Diagnostic method	Species quantification	Uncertainty source, % error	RMS error, %
Foust et al. [5]	Single element shear (GH_2/GO_2)	13	Raman spectroscopy	Mole fraction of H_2O, H_2, and O_2	Nonlinear temperature dependence of Stokes band factor (40)	40
Foust et al. [6]	Single element shear, swirl (GH_2/GO_2)	13–69	Raman spectroscopy	Mole fraction of H_2O, H_2, and O_2	1) Laser pulse energy fluctuation (5) 2) Nonlinear variation of Stokes band factor (45)	45
Brummund et al. [7]	Single element shear (LOX/GH_2)	20	PLIF	OH distribution in signal intensity	——	——
Mayer et al. [8]	Single element shear (LOX/GH_2)	15–100	Shadowgraph, flame emissions	Signal intensity (qualitative)	——	——
Yeralan et al. [9]	Single element swirl (LOX/GH_2)	28	Raman spectroscopy	Mole fraction of H_2O, H_2 and O_2	Calibration measurements (40)	40
Wehrmeyer et al. [10]	Single element swirl (LOX/GH_2)	60	Raman spectroscopy	H_2O, O_2, and H_2 distribution in signal intensity	——	——
Herding et al. [11]	Single element shear (LOX/GH_2)	10	OH emissions	Signal intensity (qualitative)	——	——
Candel et al. [12]	Single element shear (LOX/GH_2)	10	PLIF for OH and O_2.	Signal intensity (qualitative)	——	——
Ivancic et al. [13]	Single element shear (LOX/GH_2)	60	OH emissions	Signal intensity (qualitative)	——	——
Juniper et al. [14]	Single element shear (LOX/GH_2)	70	OH emissions	Signal intensity (qualitative)	——	——
Mayer et al. [15]	Single element shear (LOX/GH_2)	20–60	Shadowgraph, flame emissions	Signal intensity (qualitative)	——	——
Kalitan et al. [16]	Single element swirl (LOX/CH_4)	41	OH-PLIF and OH emissions, CO_2 emissions	Signal intensity (qualitative)	——	——
Singla et al. [17]	Single element shear (LOX/CH_4)	70	OH and CH emissions	Signal intensity (qualitative)	——	——
Singla et al. [4]	Single element shear (LOX/GH_2)	63	PLIF for OH concentration	Signal intensity (semiquantitative)	1) Boltzmann fraction variation (10) 2) Laser absorption by OH (10–30)	32
Singla et al. [18]	Single element shear (LOX/CH_4)	25–30	PLIF for OH visualization	Signal intensity (qualitative)	——	——
Smith et al. [19]	Single element shear (LOX/GH_2)	40–60	Shadowgraph, OH emissions	Signal intensity (qualitative)	——	——
Lux and Haiden [20]	Single element shear (LOX/CH_4)	40–60	OH emissions	Signal intensity (qualitative)	——	——
Lux and Haiden [21]	Single element shear (LOX/CH_4)	40–60	OH and CH emissions	Signal intensity (qualitative)	——	——

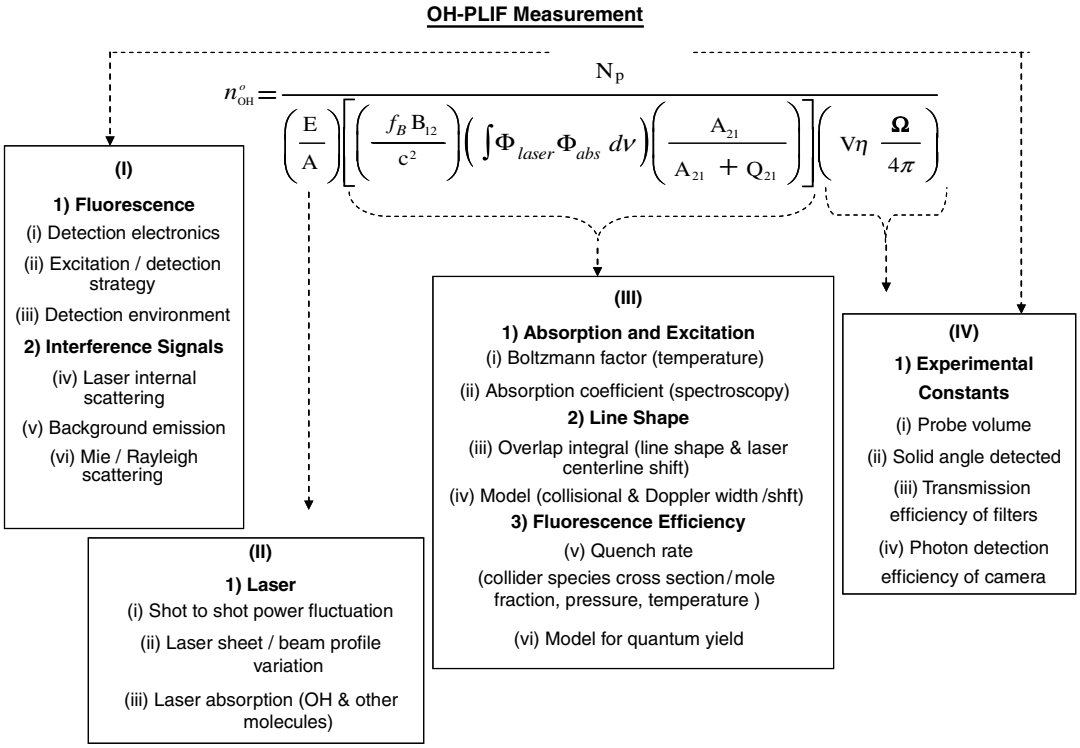

Fig. 1 Physical significance of the terms in OH number density expression based on fluorescence modeling, experimental, and quantification.

traverses through the flame due to absorption by OH and other species. All these factors contribute to the measurement uncertainties.

Furthermore, the Boltzmann fraction f_B in the initial state population $n^0 f_B$ varies with temperature and hence a careful selection of rovibrational transitions with minimum temperature dependence is recommended for PLIF diagnostics. The dependence of Φ_{abs} with temperature and pressure is to be accounted for species quantification. The determination of fluorescence yield in Eq. (1) also requires the knowledge of colliding species mole fraction in addition to temperature and pressure fields.

The strength of the fluorescence signal detected depends on the intersection volume of laser beam/sheet with the flame known as the probe volume and the fraction of solid angle collected. To avoid the interference signals and elastic scattering, optical filters are employed while collecting fluorescence; however, most of the optical filters have transmission efficiency of less than 60% at 310 nm where the OH fluorescence is detected. In addition, the photon detection efficiency at 310 nm for an ICCD camera is less than 25%. All these factors reduce the strength of the detected fluorescence signal. Thus, each step in the measurement and analysis involves uncertainties; they are addressed, identified as random or systematic, and evaluated in the detailed uncertainty analysis.

In the current study, the relative uncertainties in the parameters involved in determination of OH concentration was calculated as the ratio of the maximum variation, typically obtained as standard deviation in the parameters to their respective mean values. Systematic error sources, which depend on the local flame conditions such as temperature and mole fraction of colliding species, and the difficulty to provide an environment with accurately controllable OH concentration serve as the major difficulties for calibration [27]. The immediate consequence can be viewed as the limitations in statistical analysis of OH concentration measurements in the absence of a thorough calibration. As OH concentration determined in the study was not based on calibration, the statistical analysis is limited to parameters with random fluctuations in their measurements. In the current study, the two major random errors based on measurements included the laser shot-to-shot power fluctuation and the shot-to-shot laser sheet spatial intensity fluctuation.

B. Experimental Facility and Instrumentation

A high-pressure combustion experimental facility with a single shear GH_2/GO_2 injector was used in this study. The facility, described in detail in [31], can operate at pressures up to 60 bar. The chamber configuration and injector details are shown schematically in Fig. 2. The oxidizer is injected into the chamber through the center tube while the fuel is injected through the annular region surrounding it. The nominal pressures were selected to be in 10–55-bar range. The GH_2/GO_2 experimental conditions investigated in the current study are listed in Table 2. The oxidant to fuel mass ratio O/F as well as the

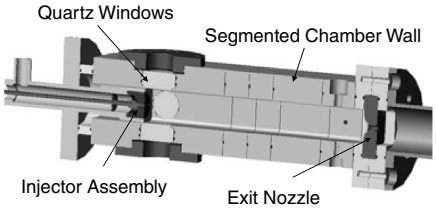

a) Combustion chamber

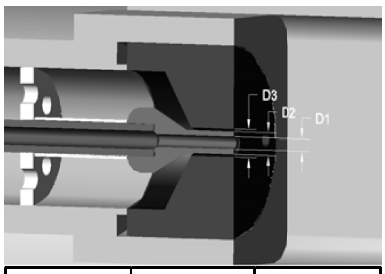

D1 (mm)	D2 (mm)	D3 (mm)
1.2	2.2	2.69

b) Injector details

Fig. 2 Experimental setup, including a) chamber geometry (the chamber is a square with 2.5 x 2.5 cm^2 cross section; the windows are uncooled and flush with the surface), and b) injector details.

Table 2 Experimental operating conditions

P, bar	O/F mass flow	O/F velocity	H_2 mass flow, g/s	H_2 velocity, m/s
10	3.77	0.39	0.197	130
27	3.72	0.39	0.395	96.5
37	3.79	0.40	0.58	103.5
53	3.85	0.40	0.75	93.4

velocity ratio were maintained the same. These two parameters are primarily responsible for the development of the shear layers, hence, mixing among the two flows. Mass flows increased as the pressure increased from one condition to the other. The experiments lasted for 8–10 s following ignition. Data were taken toward the end of the sequence when the pressure in the chamber reached essentially steady state.

The schematic of the OH-PLIF diagnostic setup is shown in Fig. 3. The third harmonic output at 355 nm from a Nd-YAG (Continuum Surelite II) pulsed laser was used to pump an optical parameter oscillator (OPO) (Continuum Panther). The full width at half-maximum spectral width of the OPO output beam, measured using a Burliegh WA-4500 wave meter, was 5 cm^{-1} and the centerline wavelength of the laser before doubling was 566.03 nm. A frequency doubler was then used to obtain a UV beam at 283 nm. The laser beam at 283 nm was formed into a sheet of 4×0.04 cm cross section using a series of fused silica lenses. Only the central portion of the laser sheet with cross section of 2×0.04 cm was used for diagnostics. The UV sheet with 2×0.04 cm cross section had a measured pulse energy of 0.89 ± 0.1 mJ and was used to excite the OH A-X(1,0) rovibrational transitions. The laser shot-to-shot power fluctuation was monitored for 290 pulses and contributes to random error. The average of the 290 laser pulse energies was 0.89 mJ/pulse with a standard deviation of 0.10 mJ/pulse and accounted for an uncertainty of 11% in laser power.

Fluorescence images were collected perpendicular to the direction of laser beam propagation using an ICCD camera (Cooke Corp. DiCam-Pro) equipped with 105 mm/4 telephoto UV lens and with quantum efficiency of 12% at 310 nm. The laser and the camera were synchronized using a pulse generator (Stanford Research Systems DG 535) and were operated at 10 Hz. The camera was used in double shutter mode such that it collected fluorescence for 100 ns in synchronization with the laser in the first image. The second image was collected 500 ns after the first image for another 100 ns to capture instantaneous flame emissions. The phosphor used in the ICCD camera was P46. The intensity decays to less than 10% in 500 ns. The maximum signal levels recorded were 10 times the dark background in this study. Hence, the decay of the signal to less than 10% of the peak intensity will not be detected by the camera as it is less than the level of the dark background. The effective resolution of the camera was 66 μm/pixel in 4×4 binning mode. Thus, the delay of 500 ns between two double shutter images was employed so that pixel resolution was not affected by the flow fluctuations of a jet at 100 m/s. The exposure time of 100 ns window was selected to make sure that all the fluorescence signals were collected. The effect of using a shorter duration shutter could be studied separately. When the flow velocity and the transient structures are considered, 100 ns is a very short duration in the lifetime of this flowfield even in the close proximity of the injector. A combination of 3-mm WG 305 Schott and 3-mm UG 11 filters were used to collect fluorescence from 306–320 nm while effectively blocking elastic scattering. The combined transmission efficiency of the filters was about 55% between 306 and 320 nm.

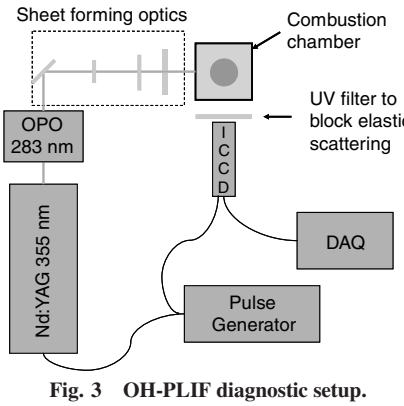

Fig. 3 OH-PLIF diagnostic setup.

OH-PLIF images were acquired for the entire run time at the rate of 10 Hz. Thirteen of the instantaneous images recorded at near steady state at the end of the experiments were averaged. The instantaneous and averaged background emission images were then subtracted from the instantaneous and averaged OH-PLIF images, respectively.

III. Oxygen/Hydrogen–Planar-Laser-Induced Fluorescence Processing: Uncertainty Assessment

The background emission images were subtracted from the fluorescence + background images. The average of 13 instantaneous images for the 37-bar case is shown in Fig. 4. The intensity levels of the background subtracted OH-PLIF images are shown in Fig. 4c. The background subtraction shown in Fig. 4 is only for the averaged images. For instantaneous OH-PLIF images, instantaneous background emission image was used for subtraction instead of averaged background emission image. The sources of the background emissions are recognized as typical flame emissions from OH and water molecules in a H_2/O_2 flame [8,15] and are potential systematic errors.

The laser sheet profile variation in space was corrected from preliminary calibration using acetone fluorescence. The laser sheet at 283 nm was passed through the chamber filled with acetone vapor, and the 2-D fluorescence was collected by effectively blocking the

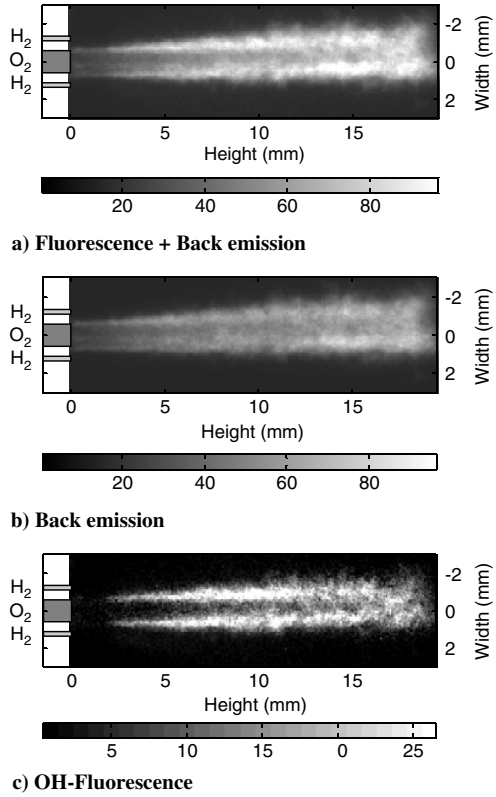

Fig. 4 Average of 13 instantaneous images obtained at near steady state for chamber pressures of 37 bar consisting of a) fluorescence+ back emission, b) back emission, and c) OH fluorescence.

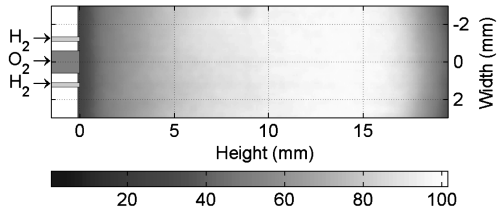

Fig. 5 Normalized laser sheet intensity profile variation obtained from acetone fluorescence images. The intensity is provided in percentage scale. The intensity is above 90% at heights of 11–15 mm and gradually decreases to 25% at heights of 1 and 19 mm.

elastic scattering using the UV filters and ICCD camera. Ninety acetone fluorescence images were averaged and normalized with the maximum intensity/counts along the width to obtain the spatial variation of the laser sheet in the region of interest. The normalized laser sheet profile variation in a percentage intensity scale is shown in Fig. 5. The laser sheet had maximum intensity of above 90% at heights of 11–15 mm, although it gradually decreased to 25% at heights of 1 and 19 mm on either side. Based on the normalized acetone fluorescence images shown in Fig. 5, the laser sheet intensity variation in space was corrected for all the OH-PLIF images acquired in the current study. The uncertainty due to the shot-to-shot fluctuation of the laser sheet spatial profile contributes to random error and was calculated as the ratio of the standard deviation to the average values of the 90 normalized acetone fluorescence images and was 5.9%.

The OH-PLIF diagnostic in this study is associated with 2-D imaging of the fluorescence on a charge-coupled device chip. Thus, the volume V (cm^3) in Eq. (1) corresponding to the collected fluorescence signal intensity in each pixel in the camera is equal to the product of the pixel projection area $A_{\text{pixel projection}}$ (cm^2) and the laser sheet thickness l (centimeters). The uncertainty associated with the volume probed is due to the accurate determination of the pixel resolution. The pixel resolution was obtained by calibrating it against the accurately known dimensions of a wire with constant diameter and length. The resultant uncertainty in the pixel resolution accounted for 2.8% uncertainty in the probe volume and is identified as systematic error. The laser sheet thickness was 400 μm and appears in the expression for laser sheet cross section area A_{laser} (cm^2) and volume probed V (cm^3). From Eq. (1), it can be seen that the laser sheet thickness cancels and does not appear in the number density expression. Hence, the error in laser sheet thickness was not considered here. Regarding the experimentally collected information, the laser sheet thickness will affect the probe volume. In these studies, the laser sheet was very carefully aligned to make sure that the sheets passed diametrically through the injector.

To obtain absolute OH concentration in number density, the arbitrary selected unit, camera counts, are to be converted to photometric units. This was done by camera calibration against a light source of known irradiance. The light source used here was a 1000-W, quartz halogen, tungsten filament lamp. The uncertainty in the irradiance levels near the 310-nm wavelength was 2.3%. The camera calibration corresponded to the detection strategy employed in the OH-PLIF measurements and region of interest. The uncertainty in the photon calibration due to the nonlinearity associated with the linear curve fit was calculated and was 1.8%. The net uncertainty in the photon calibration due to these two factors, that is, lamp irradiance uncertainty of 2.3 and 1.8% due to nonlinearity in calibration fit, accounted for 2.9% systematic error.

The uncertainty contribution from shot noise due to the Poisson distributed photon number [27] was calculated as the ratio of the standard deviation to the average photon arrival from the OH-PLIF images at 10, 27, 37, and 53 bar and is identified as random error. This uncertainty contribution accounted for 6.9, 7.05, 6.8, and 6.7%, respectively, for the four selected pressures.

The camera has spatial variation of pixel intensities and contributes to both systematic and random errors. The systematic and random spatial variation is eliminated by linear filtering, also referred to as pixel smoothening, in which the value of an output pixel in the image is computed as a weighted average of neighboring pixels [11]. In the current study, each pixel value was computed as a weighted average of the neighboring 5×5 matrix of pixels with equal weights. The uncertainty due to systematic and random spatial variation of pixel intensities, minimized by linear filtering [11], in which the value of an output pixel in the image is computed as a weighted average of neighboring pixels, was calculated as the ratio of the difference in pixel intensities before and after filtering to their corresponding averaged values. The uncertainty contribution due to pixel smoothening of the OH-PLIF images at 10, 27, 37, and 53 bar accounted for 7, 7, 6.3, and 6%, respectively.

IV. Quantification of Oxygen–Hydrogen Concentration

The OH-PLIF images were image-processed to 1) eliminate background emissions, 2) correct for spatial variation in laser intensity, and 3) pixel smoothen the images. The intensity levels of the image-processed OH-PLIF images are related to the number density of OH by Eq. (1).

To determine the number density from the image-processed OH-PLIF images, the values of absorption coefficient

$$\sum_{1}^{9} f_B B'_{12}$$

overlap integral $\int \Phi_{\text{laser}} \Phi_{\text{abs}} \, d\nu$, and collisional quench rate Q_{21} in Eq. (1), which vary with the conditions in the flame, are identified as potential sources of systematic errors and are calculated as follows. A broad range of equivalence ratios for GH_2/GO_2 combustion, 0.5–3, was considered [32]. As the OH radical exists mostly in the region of stoichiometry [3], the equivalence ratio range of 0.5–3 could be considered as an overestimation of the range of conditions in the flame. Therefore, this assumption is quite conservative and is expected to yield a larger uncertainty than actually encountered in the experiment. However, given the lack of specific inflow data, it has been adopted here to bracket with confidence the possible experimental uncertainty. In a first approximation, equilibrium conditions are assumed. The equilibrium conditions for the chemical reactions pertaining to the GH_2/GO_2 experiments were calculated using STANJAN [33]. It was found that the temperature could vary between 2500 and 3500 K, with the maximum at stoichiometry.

The variation of

$$\sum_{1}^{9} f_B B'_{12} \quad \text{cmJ}^{-1}$$

with temperature, which in turn varies with the equivalence ratio, was calculated and the mean value of

$$\sum_{1}^{9} f_B B'_{12}$$

was used to determine OH number density. The uncertainty due to the absorption coefficient variation with temperature and with respect to the mean at 10, 27, 37, and 53 bar was found as 12.4, 14.6, 14.5, and 15.1%, respectively.

The absorption profiles of OH at 10, 27, 37, and 53 bar were simulated using LIFBASE [28]. To simulate the absorption profile Φ_{abs}, the collisional and Doppler widths were calculated as described in literature [27,29]. The OH absorption profiles at 10, 27, 37, and 53 bar were simulated for a broad temperature range of 2500–3500 K corresponding to the equivalence ratio of 0.5–3. The absorption profile of OH at 3000 K in the 10–50-bar range along with the laser spectral profile is shown in Fig. 6. The OH absorption profile broadens and the centerline of the OH absorption profile shifts with pressure and temperature. The overlap integral of the absorption profile of OH at 10, 27, 37, and 53 bar, and the Gaussian spectral laser

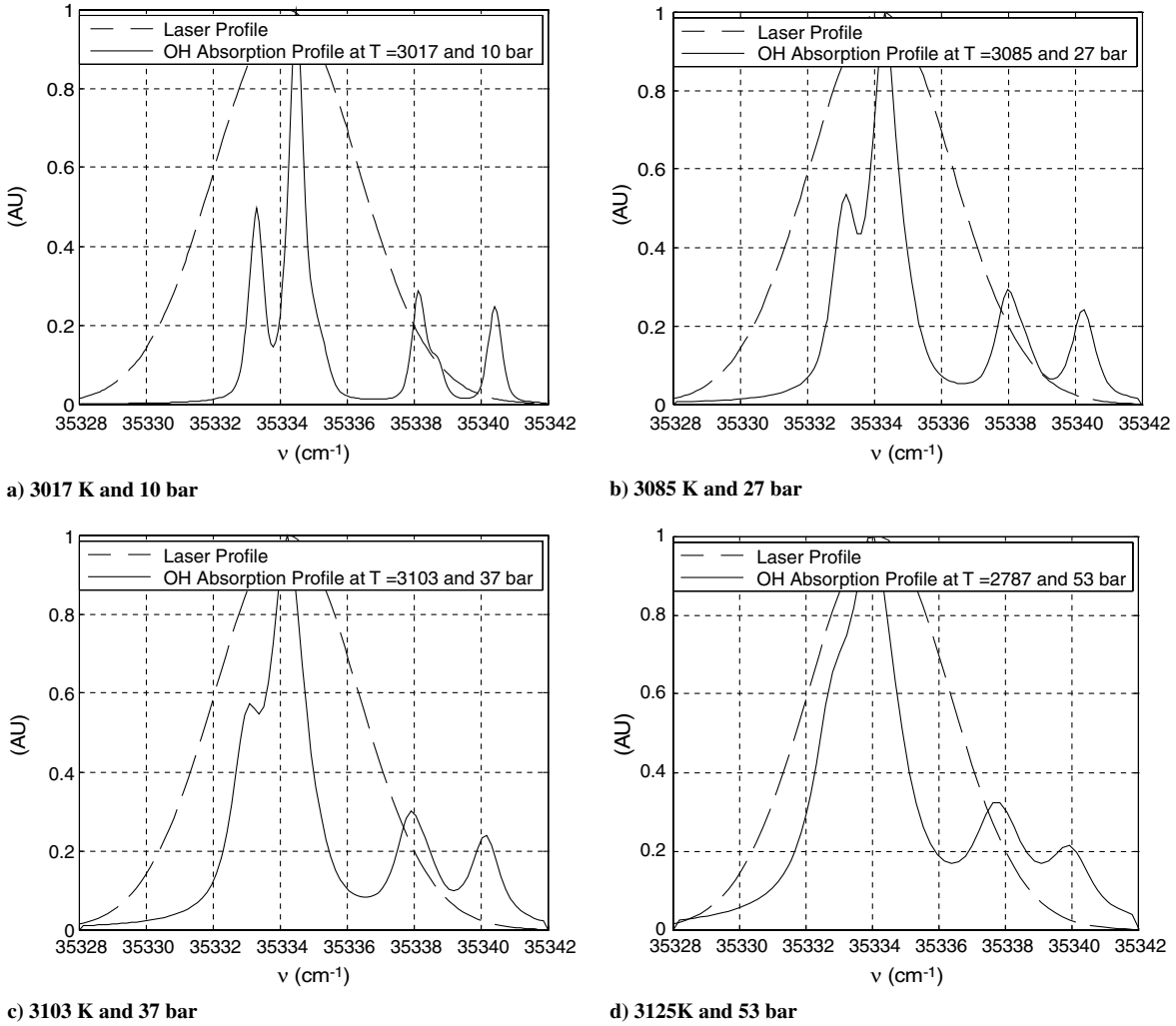

Fig. 6 Absorption profile of OH at a) 3017 K and 10 bar, b) 3085 K and 27 bar, c) 3103 K and 37 bar, and d) 3125 K and 53 bar, simulated using LIFBASE [28] showing a complete overlap with the laser spectral profile at all pressures.

profile Φ_{laser} is calculated by $\int \Phi_{laser}\Phi_{abs}\,d\nu$. As a result of the variation of the absorption profile with temperature, the determined overlap integral also varies for each pressure case over the broad range of temperature in the flame. To find this variation, the overlap integral was calculated for a temperature range of 2500–3500 K corresponding to an equivalence ratio of 0.5–3 at 10, 27, 37, and 53 bar. The resulting uncertainty due to this factor was found as 1.3, 1, 0.8, and 0.5%, respectively, for the four pressures tested over the broad temperature range of 2500–3500 K and can be, therefore, assumed negligible. The overlap integral could also vary due to the centerline shift of the laser profile. The centerline was measured as 283.015 nm. The uncertainty in the overlap integral variation at 10, 27, 37, and 53 bar due to the laser centerline shift accounted for 2.8, 1.6, 1, and 0.2%, respectively. The absorption profile broadens and gets shifted as pressure increases. Hence, in most of the studies carried out using lasers with small spectral widths of less than 1 cm^{-1}, the centerline wavelength of the laser needs to be shifted to overlap with the centerline wavelength of the OH absorption profile. The overlap between the laser spectral profile and the pressure broadened absorption profile decreases, leading to a decrease in the strength of the collected fluorescence signal as the pressure increases.

The spectral width of the laser employed in this study was larger than the spectral width of the broadened absorption profile even at elevated pressures such as 37 and 53 bar and is evident from Fig. 6. This ensured that the laser profile overlapped with the absorption profile at all pressures, thereby ensuring fluorescence with good signal strengths.

The variation of the collisional quench rate was calculated for the broad range of conditions in the flame. The mean value of the variation of Q_{21} was used to calculate fluorescence yield in Eq. (1). The uncertainty due to the variation of Q_{21} at 10, 27, 37, and 53 bar with temperature and colliding species mole fraction corresponding to equivalence ratio of 0.5–3 and with respect to mean is 4.1, 3.9, 3.8, and 3.7%, respectively.

The parameters in Eq. (1) required for determination of OH number density were determined and the image-processed OH-PLIF images were converted into absolute concentration. Figure 7 shows instantaneous and averaged OH concentration at 10, 27, 37, and 53 bar, respectively.

To present the data in mole fraction, one has to divide the number density by P/kT, where P is the pressure, k is the Boltzmann constant, and T is the temperature. The temperature is not known and, thus, the number density is considered a better indicator. As highlighted in Table 1, the absolute OH concentration data at high pressures are scarce and hence the magnitude of OH number density obtained in the current study could not be compared with other studies. Future CFD analysis could provide computed OH number densities that can be compared to those measured here.

The uncertainty due to laser absorption by OH creating a horizontal incident photon flux gradient, estimated from the average OH number density using Beer–Lambert's law [27], for a 1-mm path length of the laser at 10, 27, 37, and 53 bar was 2, 3.3, 3.8, and 4.7%, respectively. The absorption of laser by molecules contributes to systematic errors. The instantaneous results can be used for large-eddy-simulation-based codes; the averaged images are useful for

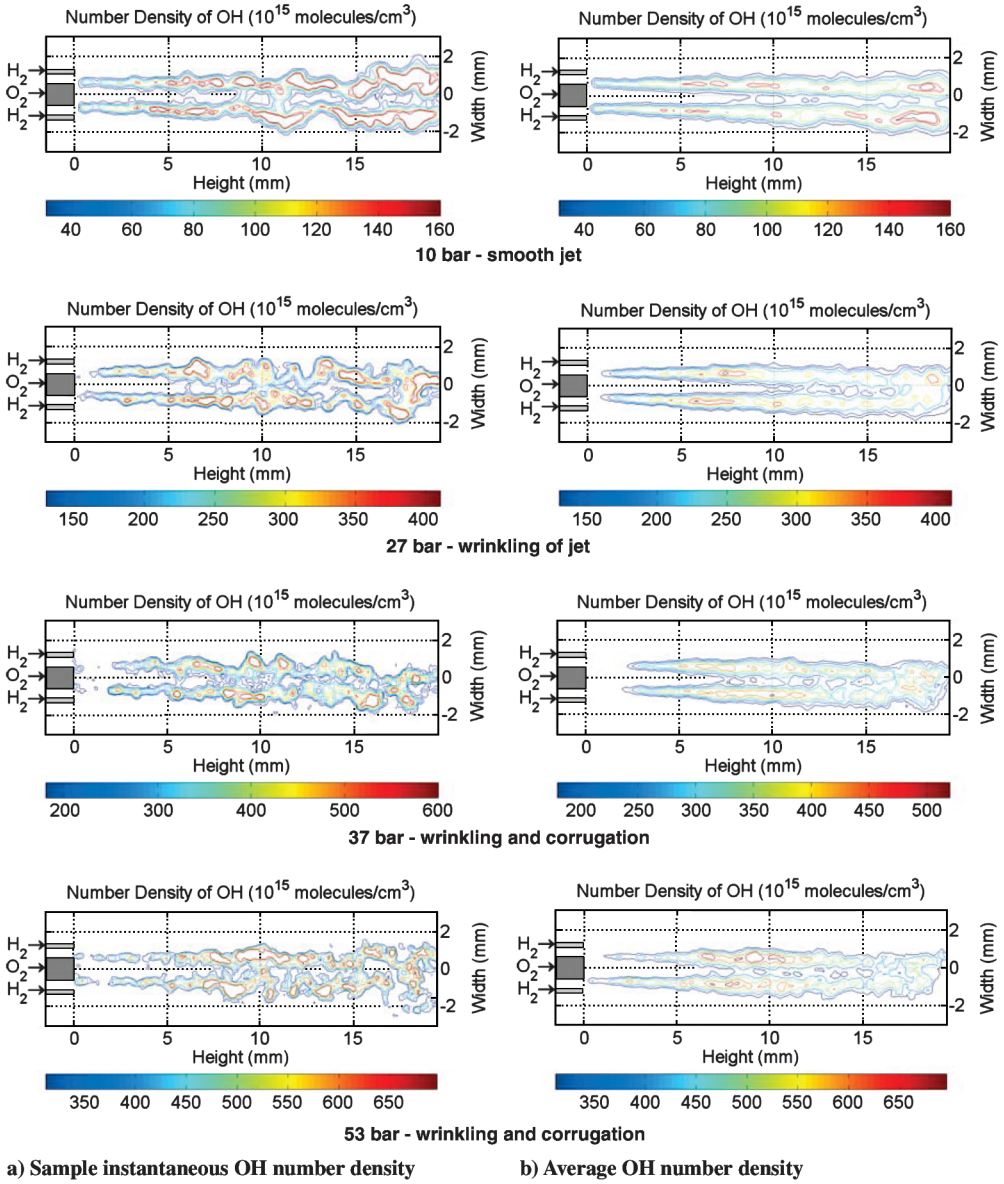

Fig. 7 OH number density contours: a) instantaneous, and b) average of 13 instantaneous contours at near steady chamber pressure of 10, 27, 37, and 53 bar, respectively.

Reynolds-averaged Navier–Stokes-based codes [1]. These results are discussed next.

V. Flame Structure

The OH number density contours in Fig. 7 show certain noteworthy features. It can be observed from the 10-bar case contours that the flame is smooth and less corrugated than is seen at higher pressures. For the four experimental conditions, O/F velocity and density ratios, which are largely responsible for the development of shear layers, remained the same. The difference in the four experiments is the turbulence and the heat release levels. In addition, Soret and Dufour cross-diffusion effects arising from concentration and temperature gradients may also play a role. These secondary effects could be effectively evaluated in complimentary CFD studies. As noted, the OH radical in a nonpremixed flame is considered to be a good marker of the reaction zone. Similar to the study described in [3], the stoichiometric contour was traced from the axial evolution of the location of maximum OH number density in the flame, as indicative of the mean position of the reaction zone. Thus, from all four average OH density contours shown in Fig. 7, the mean position of the reaction zone was quantitatively determined and is shown in Fig. 8. The mean position of the reaction zone at 10 bar shows that the flame is anchored at the lip of the oxidizer post, as is typical of the coaxial shear flames [4].

For test cases at higher pressures of 27 and 37 bar, the OH-PLIF signal would indicate a lifted flame, however, this is an effect of strong background correction in these images; in all cases, the flame was anchored at the lip. The uncertainty of 23% in OH number density refers to the maximum uncertainty at each point where OH concentration is determined, as the contour plots in Fig. 7 show. It should be noted that the 23% uncertainty has no significance at points in the flame where OH concentration cannot be determined and is therefore not provided as part of data generation.

The location of the maximum OH concentration is similar for all cases, explaining the similar effect of same density and velocity ratio on shear layer development regardless of the difference in turbulence and heat release rates.

To analyze the effect of turbulence, the Reynolds number of GO_2 and GH_2 were calculated as $\rho U D_1/\mu$ and $\rho U(D_3 - D_2)/\mu$, where ρ is the density, U is the velocity, and μ is the dynamic viscosity of the gas, and D1, D2, and D3 are the dimensions of the injector as shown in Fig. 2, respectively. The Reynolds number Re_D for GO_2 was 38,100; 75,380; 112,767; and 148,637, and for GH_2, Re_D was 5752;

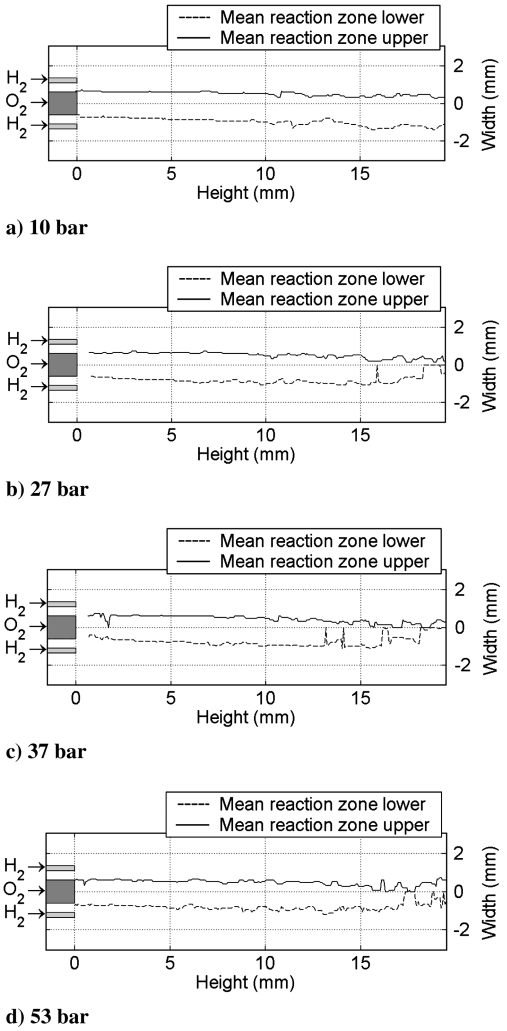

Fig. 8 Mean position of reaction zone determined from the average OH number density contours at a) 10, b) 27, c) 37, and d) 53 bar. The flame is anchored at the lip for all conditions. The flame position is same for all cases because the O/F velocity and density ratio governing shear layer development is the same.

11,534; 16,936; and 21,900 at 10, 27, 37, and 53 bar, respectively. The Re_D of GH_2 and GO_2 clearly indicate that the flow regime is turbulent. The momentum flux ratio, defined as

$$J = \frac{(\rho U^2)_{GH_2}}{(\rho U^2)_{GO_2}}$$

governs the growth of the shear layer and remained the same, $J = 0.4$, for all cases. In the study by Seitzman et al. [2], the OH structures in turbulent nonpremixed hydrogen flame were characterized at Re_D of 2300, 8600, 25,000, and 49,500. It was found that, as the flow makes the transition from laminar to the turbulent regime, there is a significant change in the OH structures from low strain rate, thick filament zones to high strain rate, thin filament, more diffuse regions. Another notable observation was that, at higher Reynolds number, the OH structures became increasingly convoluted; a similar behavior was observed in the current study, as well.

Previous studies focused on shear coaxial cryogenic flames [4,11–13,17,18] identified the wrinkling, corrugation, and flapping of the flame to be caused by the combined effects of turbulence and instabilities in the flowfield. The stability criteria based on the ratio of oxidizer lip thickness to the flame thickness greater than unity for a stable flame is discussed in detail in the literature [4,18,34]. As the flame anchors on the oxidizer lip, the size and dynamics of the recirculation region in the lip wake influences the flame stability. Thus, in the current study, the wrinkling and corrugation of the flame, at higher pressures with higher Reynolds number, is attributed to the increased turbulence, whereas the flapping of the flame, observed from the instantaneous OH distributions, is attributed to the instability dictated by two factors: 1) the size of the recirculation zone in the wake of oxidizer lip and 2) the large-scale flow fluctuation in the recirculation region formed on the injection face around the jet injectors.

VI. Discussion of Uncertainties

The summary of OH-PLIF measurement uncertainties for the 37-bar case is shown in Fig. 9.

The rms error includes the contributions from the following factors: 1) camera calibration, 2) shot noise, 3) pixel smoothening, 4) laser power variation, 5) laser spatial variation, 6) laser absorption by OH, 7) absorption coefficient, 8) overlap integral, 9) quench rate variation, and 10) pixel area accuracy. The uncertainties in the quantitative OH concentration measurements at 10, 27, 37, and 53 bar are listed in detail in Table 3.

The uncertainty due to camera calibration of 2.9%, laser shot-to-shot power fluctuation of 11%, laser sheet spatial variation of 5.9%, and pixel area of 2.8% remained the same for all the pressure cases. The uncertainties due to the laser shot-to-shot power fluctuation could be eliminated by monitoring the laser energy variation during the experiments. The uncertainty in shot-to-shot laser sheet spatial variation in intensity could be eliminated by monitoring the spatial profile during experiments from a separate calibration.

The shot noise accounted for 6–7% in all the pressure cases. The average number of photons collected in all the pressure cases was in the 200–225 range. As the pressure increases, the drop in the OH signal strength is expected due to collisional quenching. However, in the current study, the increase in the pressure was achieved by increasing the injectant mass-flow rate resulting in increased OH production at higher pressures. Thus, as the pressure increased, the strength of the collected OH signal depended mostly on the collisional quenching and increased OH production. The uncertainty due to pixel smoothening used to minimize the contribution of pixel intensity randomness in camera sensor was also 6–7% for all the pressure cases.

The study by Atakan et al. [35] covered spectroscopic measurements employing A-X(1,0) transitions in premixed methane flames from 1 to 36 bar, and the excellent agreement between the simulated and measured spectra indicated that the A-X(1,0) transition is devoid of fluorescence trapping and interference from other molecules.

Table 3 OH-PLIF uncertainties

Uncertainty source	10 bar, %	27 bar, %	37 bar, %	53 bar, %
Camera calibration		2.9		
Pixel area accuracy		2.8		
Laser shot-to-shot power fluctuation		11		
Laser sheet spatial variation		5.9		
Laser absorption (H_2O		Negligible		
Shot noise	6.9	7	6.8	6.7
Pixel smoothening	7	7	6.3	6
Laser absorption (OH)	2	3.3	3.8	4.7
Absorption coefficient temperature dependence	12.4	14.6	14.5	15.1
Overlap integral variation with absorption line shape	1.3	1	0.8	0.5
Overlap integral variation with laser centerline shift	2.8	1.6	1	0.2
Collisional quench rate variation with temperature and colliding species mole fraction	4.1	3.9	3.8	3.7
Total rms error	**21.4**	**22.8**	**22.5**	**22.9**

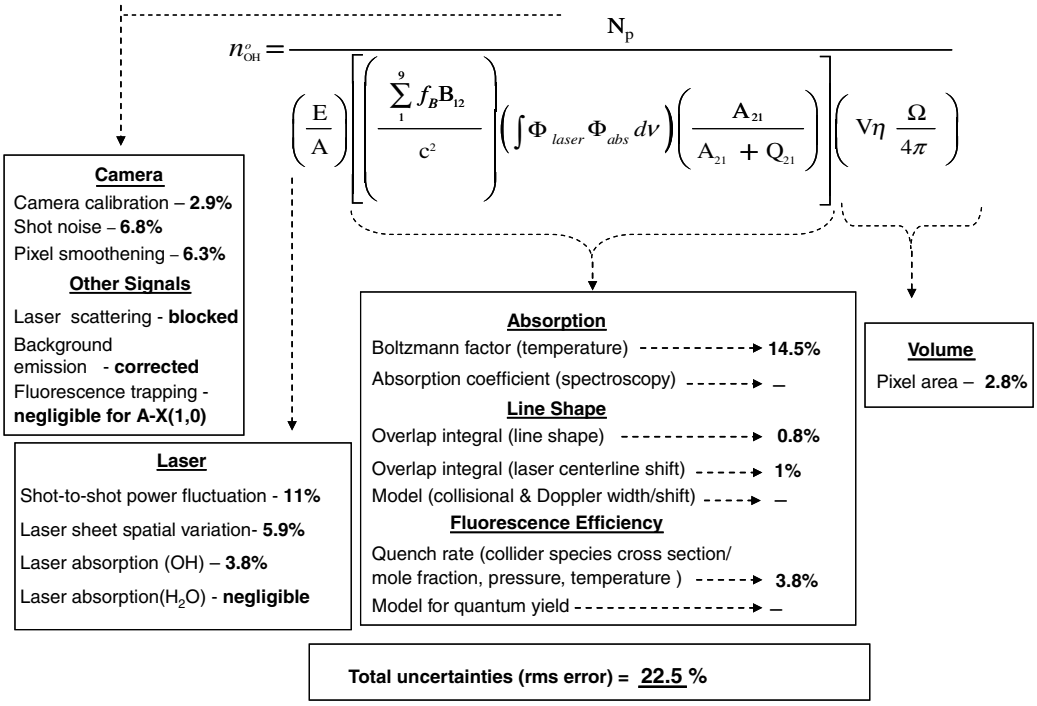

Fig. 9 OH-PLIF measurement uncertainties at 37 bar. The rms error includes the contributions from 1) shot noise, 2) pixel smoothening, 3) laser power variation, 4) laser spatial variation, 5) laser absorption by OH, 6) absorption coefficient, 7) overlap integral, 8) quench rate variation, and 9) pixel area accuracy and accounted for total rms error of 22.5%.

Hence, the effect of fluorescence trapping was considered negligible here.

The uncertainty due to the laser absorption by OH was estimated to increase from 2 to 4.7% in the 10–53-bar range. From the OH-PLIF images in Fig. 7, it could be noticed that the effect of laser absorption is negligible for all the pressure cases; this was confirmed by the uncertainty estimation.

Of all the uncertainties, the variation of the absorption coefficient with temperature was found the highest: 12–15% in the 10–53-bar range. The uncertainty due to this factor could be reduced if the 2-D temperature field is available through measurements or calculations. For flames with wrinkling, corrugation, and large fluctuations, the use of temperature field data from numerical simulation or a reference flame could lead to additional errors, as the instantaneous temperature field of the actual flame and simulated/reference flame cannot be precisely matched.

The uncertainty due to the variation of overlap integral due to line shape broadening decreased from 1.3 to 0.5% at the 10–53-bar pressure range. Similarly, the uncertainty in the overlap integral due to the shift in the centerline of the laser decreased from 2.8 to 0.2% in the 10–53-bar range. The relatively low variations in the overlap integral is attributed to the use of large laser line width of 5 cm^{-1}, thereby obtaining a complete overlap between laser spectral and OH absorption profile at all pressures, as evident from Fig. 6. Moreover, the mean value of the overlap integral was reduced by only 10% from 10 to 53 bar in the current study compared to the 30–40% reduction of overlap integral in other studies [36] due to the use of lasers with small line widths on the order of 0.5–1 cm^{-1}. The uncertainty due to variation in collisional quenching was nearly 4% in all the pressure cases and is less significant than the absorption coefficient variation of 12–15% with temperature.

The uncertainty contributions from spectroscopic constants and uncertainty in the mathematical model describing the fluorescence process, collisional/Doppler widths and shifts, and quench rate, which are identified as systematic error sources, were assumed negligible in this study. Thus, the total rms uncertainty in the OH number density measurements for a GH_2/GO_2 flame determined from a broad range of uncertainty sources accounted for 21.4, 22.8, 22.5, and 22.9% at 10, 27, 37, and 53 bar, respectively.

VII. Conclusions

This study generated a database of inflow, planar OH concentration and quantified in detail the uncertainty associated with these measurements. The oxidant/fuel mass-flow ratio was fixed at 3.77 and chamber pressures varied from 10, 27, 37, to 53 bar. Nine rovibrational lines at A-X(1,0) transition of OH and excited at 283 nm were employed to obtain OH distribution in the shear reaction zone near the coaxial injector. The quality of the inflow data assessment was improved from evaluation of two uncertainty sources in previous studies to 18 contributing factors. The information is valuable for CFD validation as it brackets the reliability of the experimental database. This study indicated the following:

1) The wrinkling, corrugation, and flapping of the flame at higher pressures of 10–27 bar was noticed and was due to the combined effects of turbulence as the Reynolds number increased and jet instability caused by size and dynamics of the recirculation region in the wake of the oxidizer postlip.

2) The errors, which remained the same irrespective of the experimental conditions, were evaluated; uncertainty due to camera calibration, laser shot-to-shot power fluctuation, laser sheet spatial variation, and pixel area accuracy was 2.9, 11, 5.9, and 2.3%, respectively. The uncertainties due to laser shot-to-shot power fluctuation and laser sheet spatial variation could be potentially minimized in future studies.

3) The uncertainty due to shot noise and pixel smoothening were each 6–7% for all the pressures cases.

4) The uncertainty due to absorption of laser across the flame by H_2O was negligible and by OH was 2–5% in the 10–50-bar range.

5) The uncertainty in absorption coefficient variation with temperature was 12–15% in the 10–50-bar range and was the maximum among all the uncertainties. This uncertainty could be potentially reduced if the temperature field data can be determined from complementary experiments or computations.

6) The uncertainty in overlap integral with temperature variation was 1.3–0.5% and 2.8–0.2% with laser centerline shift, and the mean value of overlap integral was reduced by 10% in the 10–50-bar range. The use of lasers with larger line widths is recommended for

OH-PLIF measurements at high pressures for minimizing the uncertainty due to overlap integral.

7) The uncertainty in collisional quench rate variation with temperature and colliding species mole fraction was nearly 4% at all pressures and is less significant compared to the 12–15% variation of absorption coefficient with temperature.

8) The uncertainty in the spectroscopic constants, mathematical model used to describe fluorescence process, collisional and Doppler widths, and collisional quenching are assumed negligible.

9) The total rms uncertainty contributions in OH number density analyzed and determined from 18 sources at 10, 27, 37, and 53 bar was 21.9, 22.8, 22.5, and 22.9%, respectively. To reduce the uncertainty to nearly 11% from the current 23%, potential areas for future improvements include elimination of the uncertainties due to laser power and spatial variation, and absorption coefficient variation with temperature.

Acknowledgments

This work has been performed with the support from the NASA Constellation University Institute Project. We thank Claudia Meyer, Program Manager. The authors would like to acknowledge the continuous support offered by K. Tucker (NASA Marshall Space Flight Center) and J. Hulka (Jacobs Sverdrup).

References

[1] Tucker, K., West, J., Williams, R., Lin, J., Rocker, M., Canabal, F., Robles, B., and Garcia, R., "Using CFD as a Rocket Injector Design Tool: Recent Progress at Marshall Space Flight Center," NASA TR 20030112990, Oct. 2003.

[2] Seitzman, J. M., Ungut, A., Paul, P. H., and Hanson, R. K., "Imaging and Characterization of OH Structures in a Turbulent Non-Premixed Flame," *Proceedings of the Combustion Institute*, Vol. 23, 1990, pp. 637–644.

[3] Theron, M., and Bellenoue, M., "Experimental Investigation of the Effects of Heat Release on Mixing Processes and Flow Structure in a High Speed Subsonic Turbulent H_2 Jet," *Combustion and Flame*, Vol. 145, No. 4, 2006, pp. 688–702. doi:10.1016/j.combustflame.2006.01.012

[4] Singla, G., Scouflaire, P.,Rolon, C., and Candel, S., "Planar Laser-Induced Fluorescence of OH in High Pressure Cryogenic LOX/GH_2 Jet Flames," *Combustion and Flame*, Vol. 144, Nos. 1–2, 2006, pp. 151–169. doi:10.1016/j.combustflame.2005.06.015

[5] Foust, M. J., Deshpande, M., Pal, S., Ni, T., Merkle, C. L., and Santoro, R. J., "Experimental and Analytical Characterization of a Sheer Coaxial Combusting GO2/GH2 Flowfield," AIAA Paper 96-0646, Jan. 1996.

[6] Foust, M. J., Pal, S., and Santoro, R. J., "Gaseous Propellant Rocket Studies Using Raman Spectroscopy," AIAA Paper 96-2766, July 1996.

[7] Brummund, U., Cassou, A., and Vogel, A., "PLIF Imaging Measurements of a Coaxial Rocket Injector Spray at Elevated Pressure," *Proceedings of the Combustion Institute*, Vol. 26, 1996, pp. 1687–1695.

[8] Mayer, W., and Tamura, H., "Propellant Injection in a Liquid Oxygen/Gaseous Hydrogen Rocket Engine," *Journal of Propulsion and Power*, Vol. 12, No. 6, 1996, pp. 1137–1147. doi:10.2514/3.24154

[9] Yerlan, S., Pal, S., and Santora, R. J., "Major Species and Temperature Profiles of LOX/GH2 Combustion," AIAA Paper 97-2974, July 1997.

[10] Wehrmeyer, J. A., Cramer, J. M., Eskridge, R. H., and Dobson, C. C., "UV Diagnostics for Rocket Engine Injector Development," AIAA Paper 97-2843, July 1997.

[11] Herding, G., Snyder, R., Rolon, C., and Candel, S., "Investigation of Cryogenic Propellant Flames Using Computerized Tomography of Emission Images," *Journal of Propulsion and Power*, Vol. 14, No. 2, 1998, pp. 146–151. doi:10.2514/2.5279

[12] Candel, S., Herding, G., Synder, R., Scouflaire, P., Rolon, C., Vingert, L., Habiballah, M., Grisch, F., Pealat, M., Bouchardy, P., Stepowski, D., Cessou, A., and Colin, P., "Experimental Investigation of Shear Coaxial Cryogenic Jet Flames," *Journal of Propulsion and Power*, Vol. 14, No. 5, 1998, pp. 826–834. doi:10.2514/2.5346

[13] Ivancic, B., Mayer, W., Krulle, G., and Bruggemann, D., "Experimental and Numerical Investigation of Time and Length Scales in LOX/GH_2-Rocket Combustors," AIAA Paper 99-2211, June 1999.

[14] Juniper, M., Tripathi, A., Scouflaire, P., Rolon, J.-C., and Candel, S., "Structure of Cryogenic Flames at Elevated Pressures," *Proceedings of the Combustion Institute*, Vol. 28, 2000, pp. 1103–1109.

[15] Mayer, W., Schik, A., and Schaffler, M., "Injection and Mixing Process in High Pressure Liquid Oxygen/Gaseous Hydrogen Rocket Combustors," *Journal of Propulsion and Power*, Vol. 16, No. 5, 2000, pp. 823–828. doi:10.2514/2.5647

[16] Kalitan, D. M., Salgues, D., Mouis, A. G., Lee, S. Y., Pal, S., and Santoro, R. J., "Experimental Liquid Rocket Swirl Coaxial Injector Study Using Non-Intrusive Optical Techniques," AIAA Paper 2005-4299, June 2005.

[17] Singla, G., Scouflaire, P., Rolon, C., and Candel, S., "Transcritical Oxygen/Transcritical or Supercritical Methane Combustion," *Proceedings of the Combustion Institute*, Vol. 30, 2005, pp. 2921–2928.

[18] Singla, G., Scouflaire, P., Rolon, J. C., Candel, S., and Vingert, L., "OH Planar Laser-Induced Fluorescence and Emission Imaging in High-Pressure LOX/Methane Flames," *Journal of Propulsion and Power*, Vol. 23, No. 3, 2007, pp. 593–602. doi:10.2514/1.24895

[19] Smith, J. J., Schneider, G., Suslov, D., Oschwald, M., and Haidn, O., "Steady-State High Pressure LOX/H_2 Rocket Engine Combustion," *Aerospace Science and Technology*, Vol. 11, No. 1, 2007, pp. 39–47. doi:10.1016/j.ast.2006.08.007

[20] Lux, J., and Haiden, O., "Flame Stabilization in High Pressure Liquid Oxygen (LOX)/Methane Rocket Engine Combustion," *Journal of Propulsion and Power*, Vol. 25, No. 1, 2009, pp. 24–32. doi:10.2514/1.37308

[21] Lux, J., and Haidn, O., "Effect of recess in high pressure Liquid Oxygen (LOX)/Methane coaxial injection and combustion," *Journal of Propulsion and Power*, Vol. 25, No. 1, 2009, pp. 15–23. doi:10.2514/1.36852

[22] Hanson, R. K., "Combustion Diagnostics: Planar Imaging Techniques," *Proceedings of the Combustion Institute*, Vol. 21, 1986, pp. 1677–1691.

[23] Schefer, R. W., Namazian, M., and Kelly, J., "CH, OH and CH4 Concentration Measurements in a Lifted Turbulent-Jet Flame," *Proceedings of the Combustion Institute*, Vol. 23, 1990, pp. 669–676.

[24] Battles, B. E., and Hanson, R. K., "Laser-Induced Fluorescence Measurements of No and OH Mole Fraction in Fuel-Lean, High-Pressure (1–10 atm) Methane Flames: Fluorescence Modeling and Experimental Validation," *Journal of Quantitative Spectroscopy and Radiative Transfer*, Vol. 54, No. 3, 1995, pp. 521–537. doi:10.1016/0022-4073(95)00020-L

[25] Arnold, A., Bombach, R., Kappeli, B., and Schlegel, A., "Quantitative Measurements of OH Concentration Fields by Two Dimensional Laser-Induced Fluorescence," *Applied Physics B*, Vol. 64, No. 5, 1997, pp. 579–583. doi:10.1007/s003400050218

[26] Eckbreth, A. C., *Laser Diagnostics for Combustion Temperature and Species*, 2nd ed., Vol. 3, Gordon and Breach, New York, 1996.

[27] Daily, J. W., "Laser Induced Fluorescence Spectroscopy in Flames," *Progress in Energy and Combustion Science*, Vol. 23, No. 2, 1997, pp. 133–199. doi:10.1016/S0360-1285(97)00008-7

[28] Luque, J., and Crosley, D., "LIFBASE : Database and Spectral Simulation Program, Technical Report," SRI International Rept. MP 99-009, Ver. 2.055, 1999.

[29] Davidson, D., Roehrig, M., Peterson, E., Di Rosa, and Hanson, R., "Measurements of the OH A-X (0,0) 306 nm Absorption Bandhead at 60 atm and 1735 K," *Journal of Quantitative Spectroscopy and Radiative Transfer*, Vol. 55, No. 6, 1996, pp. 755–762. doi:10.1016/0022-4073(96)00024-6

[30] Paul, P. H., "A Model for Temperature-Dependent Collisional Quenching of OH $A^2\Sigma^+$," *Journal of Quantitative Spectroscopy and Radiative Transfer*, Vol. 51, No. 3, 1994, pp. 511–524. doi:10.1016/0022-4073(94)90150-3

[31] Conley, A., Vaidyanathan, A., and Segal, C., "Heat Fluxes Measurements in a GO2/GH2 Single-Element, Shear Injector," *Journal of Spacecraft and Rockets*, Vol. 44, No. 3, 2007, pp. 633–639. doi:10.2514/1.26678

[32] Meyer, T. R., Roy, S., Belovich, V. M., Corporan, E., and Gord, J. R., "Simultaneous Planar Laser-Induced Fluorescence, OH Planar Laser-Induced Fluorescence and Droplet Mie Scattering in Swirl-Stabilized Spray Flames," *Applied Optics*, Vol. 44, No. 3, 2005, pp. 445–454. doi:10.1364/AO.44.000445

[33] Reynolds, W. C., *STANJAN: a Reaction Chemistry Computer Program*, Stanford Univ., Stanford, CA, 1987.

[34] Juniper, M., and Candel, S., "Edge Diffusion Flame Stabilization Behind a Step over a Liquid Reactant," *Journal of Propulsion and Power*, Vol. 19, No. 3, 2003, pp. 332–342. doi:10.2514/2.6134

[35] Atakan, B., Heinze, J., and Meier, U. E., "OH Laser-Induced Fluorescence at High Pressures: Spectroscopic and Two-Dimensional Measurements Exciting the A-X(1, 0) Transition," *Applied Physics B*, Vol. 64, No. 5, 1997, pp. 585–591. doi:10.1007/s003400050219

[36] Seitzman, J. M. and Hanson, R. K., "Comparison of Excitation Techniques for Quantitative Fluorescence Imaging of Reacting Flow," *AIAA Journal*, Vol. 31, No. 3, 1993, pp. 513–519. doi:10.2514/3.11359

D. Talley
Associate Editor